CHEMISTRY
A European Journal

Supporting Information

$K_2Au(IO_3)_5$ and β-$KAu(IO_3)_4$: Polar Materials with Strong SHG Responses Originating from Synergistic Effect of AuO_4 and IO_3 Units**

Xiang Xu,[a] Chun-Li Hu,[a] Bing-Xuan Li,[b] and Jiang-Gao Mao*[a]

chem_201504117_sm_miscellaneous_information.pdf

Table S1. Selected bond lengths (Å) and angles (deg) for $K_2Au(IO_3)_5$ and *β*-$KAu(IO_3)_4$.

Table S2. Calculated dipole moments for single IO_3, AuO_4, and $Au(IO_3)_4$ units, and net dipole moments for a unit cell of $K_2Au(IO_3)_5$ and *β*-$KAu(IO_3)_4$.

Figure S1. EDS results of $K_2Au(IO_3)_5$ (a) and β-$KAu(IO_3)_4$ (b).

Figure S2 Experimental and simulated powder X-ray diffraction patterns of $K_2Au(IO_3)_5$ (a) and *β*-$KAu(IO_3)_4$ (b).

Figure S3. Powder X-ray diffraction patterns of the residuals after thermal decompositions for $K_2Au(IO_3)_5$ and *β*-$KAu(IO_3)_4$ (a) compared with the simulated patterns for Au (b) and KIO_3 (c).

Figure S4. IR spectra of of $K_2Au(IO_3)_5$ (a) and *β*-$KAu(IO_3)_4$ (b).

Figure S5. The scissor-added band structures for $K_2Au(IO_3)_5$(a) and *β*-$KAu(IO_3)_4$ (b).

Figure S6. The corresponding orbital graphs of the PDOS peaks labeled by 1~6 for $K_2Au(IO_3)_5$.

Figure S7. The corresponding orbital graphs of the PDOS peaks labeled by 1~6 for *β*-$KAu(IO_3)_4$.

Table S1. Selected bond lengths (Å) and angles (deg) for $K_2Au(IO_3)_5$ and β-$KAu(IO_3)_4$. [a]

$K_2Au(IO_3)_5$			
Au(1)-O(9)	1.987(12)	Au(1)-O(6)	1.989(14)
Au(1)-O(9)$^{\#1}$	1.987(12)	Au(1)-O(4)	2.013(13)
I(1)-O(1)	1.815(19)	I(3)-O(5)	1.823(13)
I(1)-O(2)	1.828(12)	I(3)-O(5)$^{\#1}$	1.823(13)
I(1)-O(2)$^{\#2}$	1.828(12)	I(3)-O(6)	1.879(16)
I(2)-O(3)	1.796(13)	I(4)-O(7)	1.798(13)
I(2)-O(3)$^{\#1}$	1.796(13)	I(4)-O(8)	1.797(12)
I(2)-O(4)	1.900(17)	I(4)-O(9)	1.908(13)
O(4)-Au(1)-O(9)	88.4(3)	I(2)-O(4)-Au(1)	112.7(8)
O(6)-Au(1)-O(9)	91.4(4)	I(3)-O(6)-Au(1)	120.1(8)
O(4)-Au(1)-O(6)	175.5(7)	I(4)-O(9)-Au(1)	118.1(7)
O(9)-Au(1)-O(9)$^{\#1}$	173.9(8)		
β-$KAu(IO_3)_4$			
Au(1)-O(6)	1.973(5)	Au(1)-O(3)	1.992(5)
Au(1)-O(6)$^{\#1}$	1.973(5)	Au(1)-O(3)$^{\#1}$	1.992(5)
I(1)-O(1)	1.786(6)	I(2)-O(4)	1.792(6)
I(1)-O(2)	1.789(6)	I(2)-O(5)	1.799(6)
I(1)-O(3)	1.891(7)	I(2)-O(6)	1.889(6)
O(6)-Au(1)-O(3)	89.9(2)	O(6)-Au(1)-O(6)$^{\#1}$	174.3(4)
O(6)-Au(1)-O(3)$^{\#1}$	90.1(2)	O(3)-Au(1)-O(3)$^{\#1}$	180.0(4)
I(1)-O(3)-Au(1)	114.2(3)	I(2)-O(6)-Au(1)	120.3(3)

[a] Symmetry transformations used to generate equivalent atoms, for $K_2Au(IO_3)_5$: #1 -x+1, y, z; #2 -x, y, z; for β-$KAu(IO_3)_4$: #1 -x+1, y, -z+1.

Table S2. Calculated dipole moments for single IO_3, AuO_4, and $Au(IO_3)_4$ units, and net dipole moments for a unit cell of $K_2Au(IO_3)_5$ and β-$KAu(IO_3)_4$. [a]

$K_2Au(IO_3)_5$				
unit	Dipole moment (D = Debyes)			
	x-component	*y*-component	*z*-component	total magnitude
I(1)O_3	0	-0.226	13.209	13.211
I(2)O_3	0	±13.008	0.116	13.008
I(3)O_3	0	±5.966	13.775	15.012
I(4)O_3	±4.141	±11.432	7.941	14.522
AuO_4	0	±0.285	1.327	1.357
$Au(IO_3)_4$	0	±41.552	31.100	51.901
Net dipole moment (a unit cell)	0	0	177.232	177.232
β-$KAu(IO_3)_4$				
unit	Dipole moment (D = Debyes)			
	x-component	*y*-component	*z*-component	total magnitude
I(1)O_3	±13.860	0.116	±3.860	14.387
I(2)O_3	±5.246	-13.994	±4.852	15.713
AuO_4	0	-0.816	0	0.816
$Au(IO_3)_4$	0	-28.573	0	28.573
Net dipole moment (a unit cell)	0	-57.147	0	57.147

[a] *x*, *y*, and *z* represent the Cartesian coordinate system, for $K_2Au(IO_3)_5$, the *x*, *y*, and *z* are parallel to the crystallographic axis *a*, *b*, and *c*, respectively; for β-$KAu(IO_3)_4$, the *x* and *y* are parallel to *a* and *b* axis, respectively, and *z* located at the *ac* plane with deviation of 19.184 ° from the *c* axis.

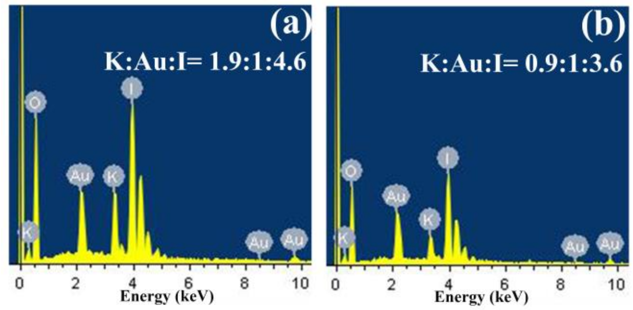

Figure S1. EDS results of $K_2Au(IO_3)_5$ (a) and β-$KAu(IO_3)_4$ (b).

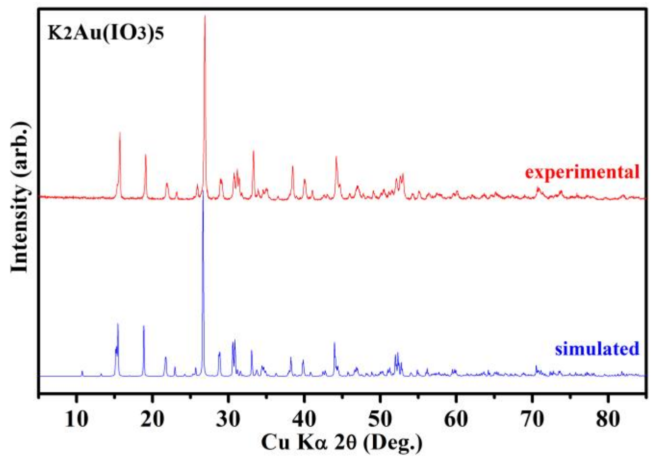

(a)

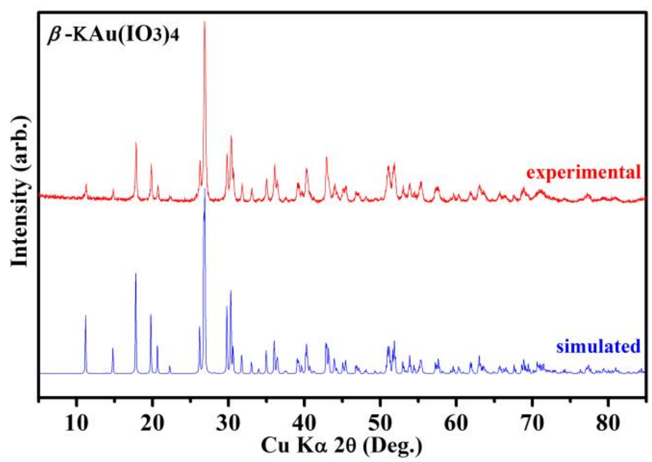

(b)

Figure S2. Experimental and simulated powder X-ray diffraction patterns of $K_2Au(IO_3)_5$ (a) and *β*-$KAu(IO_3)_4$ (b).

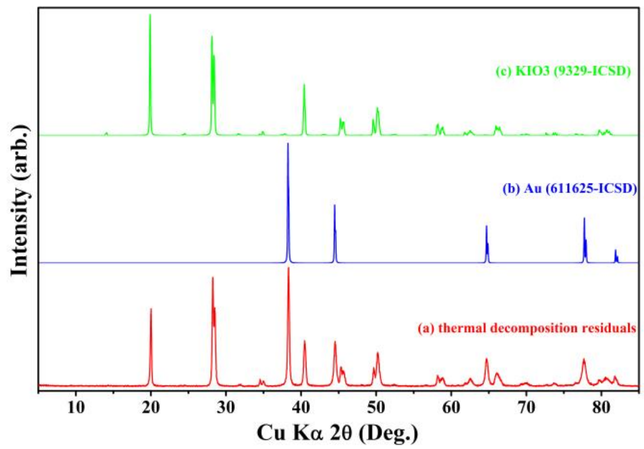

Figure S3. Powder X-ray diffraction patterns of the residuals after thermal decompositions for $K_2Au(IO_3)_5$ and β-$KAu(IO_3)_4$ compared with the simulated patterns for Au and KIO_3.

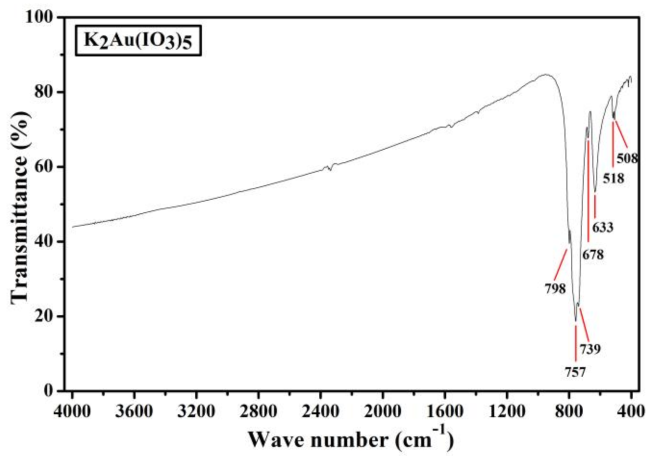

(a)

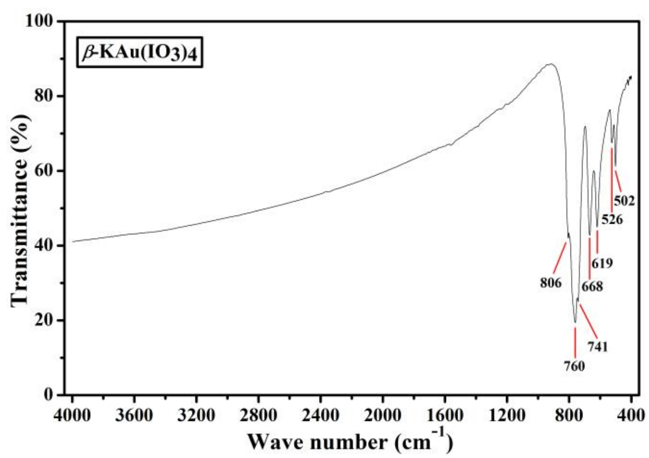

(b)

Figure S4. IR spectra of of $K_2Au(IO_3)_5$ (a) and β-$KAu(IO_3)_4$ (b).

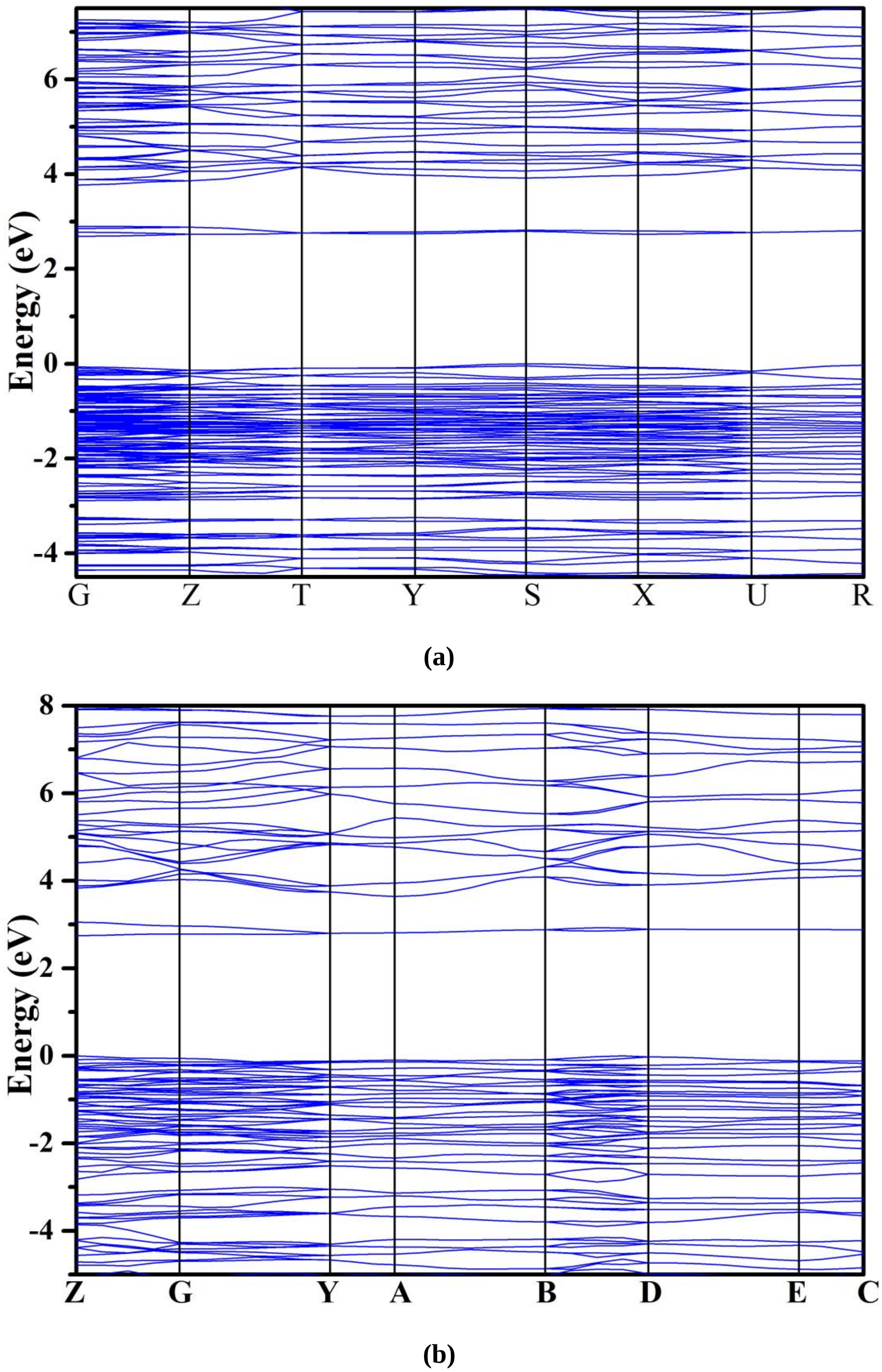

(a)

(b)

Figure S5. The scissor-added band structures for $K_2Au(IO_3)_5$(a) and β-$KAu(IO_3)_4$ (b).

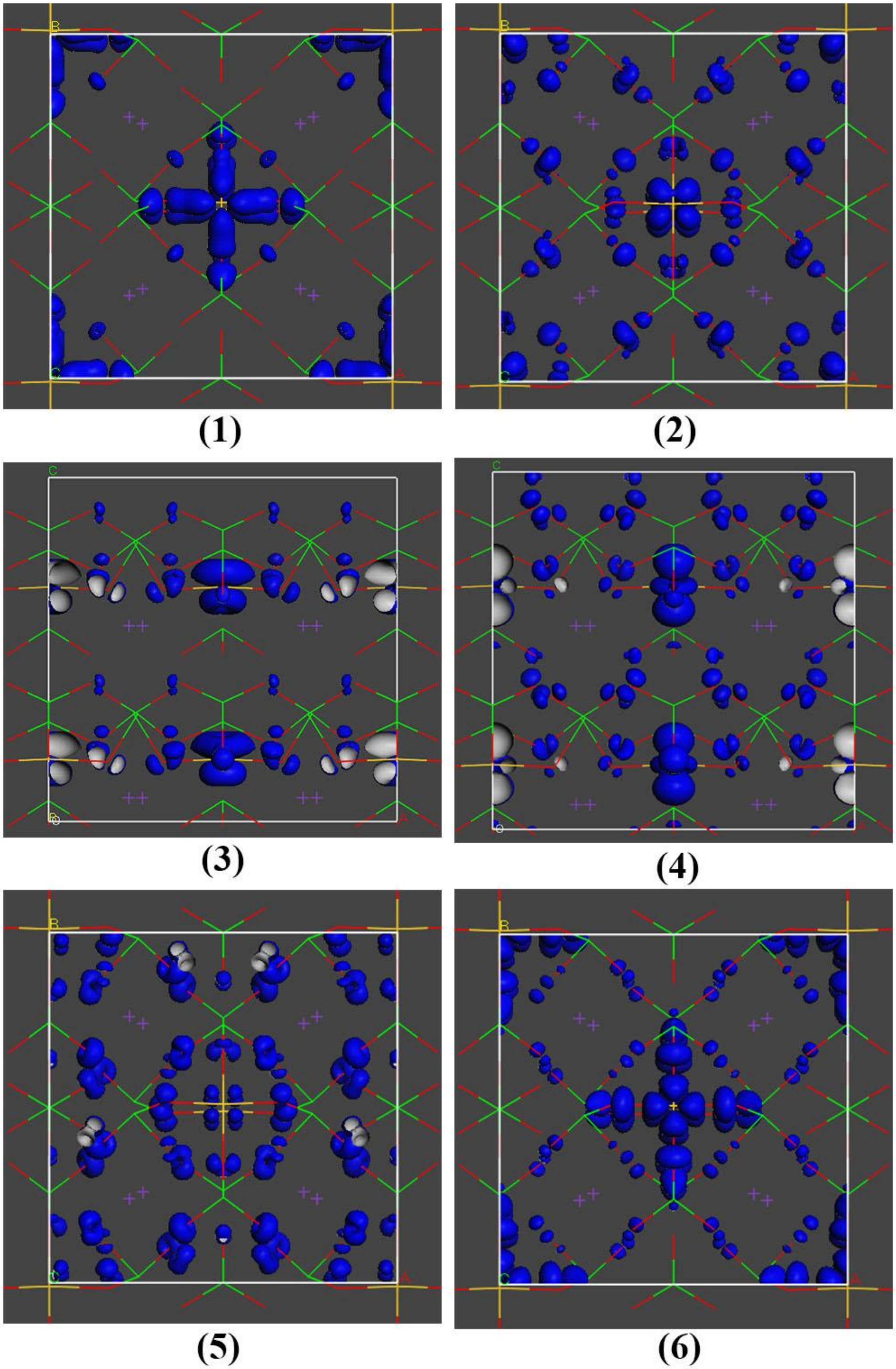

Figure S6. The corresponding orbital graphs of the PDOS peaks labeled by 1~6 for $K_2Au(IO_3)_5$.

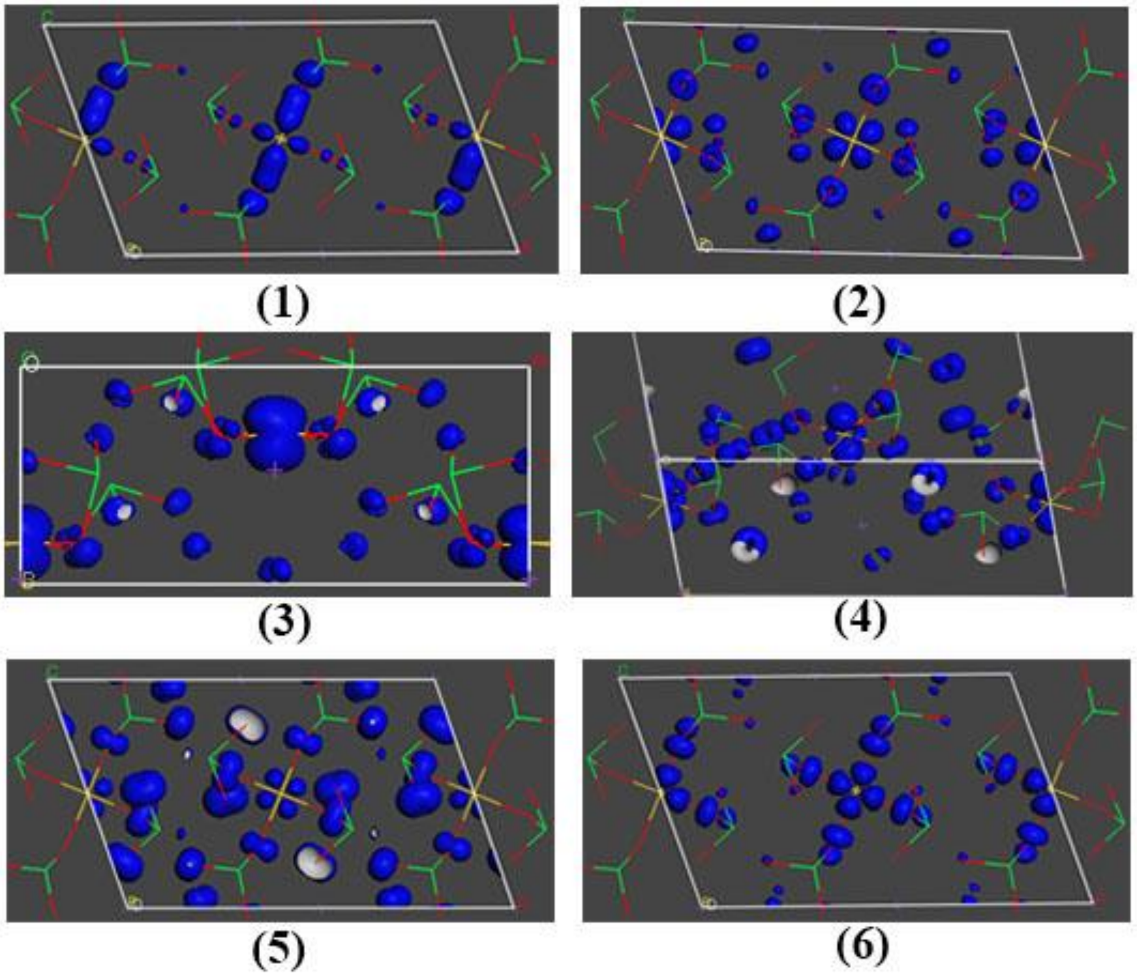

Figure S7. The corresponding orbital graphs of the PDOS peaks labeled by 1~6 for β-$KAu(IO_3)_4$.